Received: 9 July 2019 | Revised: 2 July 2020 | Accepted: 7 July 2020

DOI: 10.1111/tgis.12676

RESEARCH ARTICLE

Transactions in GIS WILEY

fusionImage: An R package for pan-sharpening images in open source software

Fulgencio Cánovas-García[1,2,3] | **Paúl Pesántez-Cobos**[4] | **Francisco Alonso-Sarría**[5]

[1]Departamento de Geografía Humana, Universidad de Sevilla, Sevilla, Spain

[2]Departamento de Geología y Minas e Ingeniería Civil, Universidad Técnica Particular de Loja, Loja, Ecuador

[3]Departamento de Ingeniería Minera y Civil, Universidad Politécnica de Cartagena, Cartagena, Spain

[4]Departamento de Ingeniería Civil, Universidad de Cuenca, Cuenca, Ecuador

[5]Instituto Universitario del Agua y del Medio Ambiente, Universidad de Murcia, Murcia, Spain

Correspondence
Fulgencio Cánovas-García, Departamento de Geografía Humana, Universidad de Sevilla, María de Padilla s/n, 41004 Sevilla, Spain.
Email: fulgencio.canovas@um.es

Funding information
Saavedra Fajardo programme, Grant/Award Number: 20023/SF/16 (Fundación Séneca-Agencia de Ciencia y Tecnología de la Región de Murcia). Grant/Award Number: CGL2017-84625-C2-2-R (Spanish Ministry of Economy, Industry and Competitiveness (MINECO), Spanish Research Agency (AEI) and European Regional Development Funds (FEDER)).

Abstract

The objective of this article is to evaluate the performance of three pan-sharpening algorithms (high-pass filter, principal component analysis and Gram–Schmidt) to increase the spatial resolution of five types of multispectral images and to evaluate the results in terms of color, coherence and spatial sharpness, both qualitatively and quantitatively. A secondary objective is to present an implementation of the aforementioned pan-sharpening techniques within the open source software R. From a qualitative point of view, pan-sharpening of images with a high spatial resolution ratio give better results than those whose spatial resolution ratio is 2. According to the quantitative evaluation, there is no pan-sharpening methodology that obtains optimal results simultaneously for all types of images used. The results of the spectral and spatial ERGAS index vary for four out of the five types of images analyzed. The results show that none of the methods implemented in this work can be considered a priori better than the others. At the same time, this work indicates the importance of both qualitative and quantitative assessment.

1 | INTRODUCTION

Image fusion has been described as a set of techniques that combine images of different spatial resolutions or containing different types of information with the objective of generating new images that enhance the properties of the originals (Liu & Mason, 2009). The overall aim is to improve the interpretability of data by improving their

Fulgencio Cánovas-García, Paúl Pesántez-Cobos and Francisco Alonso-Sarría are equally contributing authors.

visual quality, by facilitating the discrimination of certain categories, or by increasing the accuracy of subsequent analysis methods (Chuvieco, 2016). Pan-sharpening refers to the fusion of a panchromatic (PAN) and a multispectral (MS) image that have been simultaneously acquired over the same area. This can be interpreted as a particular case of data fusion as the aim is to combine the spatial details in the PAN image with the spectral bands in the MS image into one product (Vivone et al., 2015). When a PAN band is available, light is collected for a wide range of wavelengths, usually covering all MS bands. This allows the pixel size to be reduced while still maintaining the minimum intensity necessary to trigger the PAN sensor (Brodu, 2017). Image pan-sharpening tries to minimize spatial and spectral distortion in the pan-sharpened images (Zhang & Roy, 2016).

The demand for pan-sharpened data is steadily rising due to the increasing availability of commercial products that provide high-resolution spatial imagery to the general public and users such as Google Earth and Bing Maps. In addition, pan-sharpening is a type of image preprocessing used for many remote sensing tasks such as change detection, object recognition or photointerpretation (Vivone et al., 2015). It is commonly used in both environmental and social sciences; for example, to improve the interpretation of geomorphological forms (Ewertowski, Evans, Roberts, & Tomczyk, 2016) and the monitoring of urban sprawl (Huang, Wen, Li, & Qin, 2017). Another reason for image pan-sharpening is that more than 70% of terrestrial observation satellites and a large number of digital aerial cameras are simultaneously equipped with PAN and MS sensors (Zhang, 2004; Zhang & Mishra, 2012). *Landsat-8*, *GeoEye*, *OrbView*, *SPOT*, *WorldView* and *Pleiades* are examples of this configuration, enabling users to take advantage of the complementarity of data sets coming from both types of sensors. The increasing number and availability of high-resolution optical satellites as well as the ever-improving revisit cycles allow complementary high-resolution and MS images to be obtained during the same season and possibly under similar atmospheric and illumination conditions (Yokoya, Grohnfeldt, & Chanussot, 2017). Snehmani, Ganju, Kumar, Srivastava, and Hari Ram (2016) also state that pan-sharpening is one of the essential steps for improving the image quality of many remote sensing applications and that it is not obvious to non-specialists how to select one method in preference to others for a given case.

The difference in spatial resolution between the PAN and MS modes can be measured by the spatial resolution ratio (or spatial ratio), that is, the ratio of their respective ground sampling distances. Spatial ratios usually vary between 2 and 5 (Ehlers, Jacobsen, & Schiewe, 2009; Ehlers, Klonus, Astrand, & Rosso, 2010), although the most common is a spatial ratio of 2 (*Landsat ETM+* and OLI) or 4 (*IKONOS-2*, *QuickBird-2*, *GeoEye-1*, *GeoEye-2*, *Pleiades* and *WorldView-2*). The spatial resolution ratio may be even higher if data from different satellites are used (Klonus & Ehlers, 2009; Yokoya et al., 2017). Some studies have achieved acceptable results with ratios equal to or greater than 4, depending on the image characteristics and the pan-sharpening methodology used (Gangkofner, Pradhan, & Holcomb, 2008; Yuhendra, Kuze, & Sri Sumantyo, 2010; Zhang, 2002).

Several pan-sharpening algorithms have been proposed and some attempts have been made to classify them. A broader overview can be found in Pohl and Van Gendreen (1998), Darvishi Boloorani (2008) , Amro, Mateos, Vega, Molina, and Katsaggelos (2011), and Basaeed, Bhaskar, and Al-Mualla (2013). Because of the differences that exist among sensors and among the features of the Earth's surface, there is no consensus on which pan-sharpening technique provides the best results (Zhang & Roy, 2016). How to effectively evaluate the quality of the results has been a challenge to researchers and users of these fused products. However, two approaches have been widely used in research (Zhang, 2008): qualitative approaches involve the visual comparison of the original MS and the fused images to verify color coherence, and a comparison of the original PAN and the pan-sharpened images to verify that spatial detail is preserved; quantitative approaches, on the other hand, involve a set of predefined quality indicators to measure the spectral and spatial similarities between the pan-sharpened and the original (PAN and MS) images.

R is an open source statistical programming environment (R Development Core Team, 2009) in which many of the new image processing developments are being implemented because of its power, flexibility, and community of developers and users, among other reasons. The use of R has increased, not only in statistics but also as a reference program in many scientific disciplines, including geographic information science and remote sensing, with packages such as `raster` (Hijmans, 2016), `landsat` (Goslee, 2011), and `sf` (Pebesma, 2018). The `raster` package, in particular, has overcome several limitations in the handling of large images. Pebesma, Nüst, and Bivand (2012) presents some arguments as to why the R software environment is a good option for carrying out reproducible geoscientific research, and Bivand, Pebesma, and Gómez-Rubio (2013) highlight the increasing importance of geospatial analysis in R usage and development.

The objectives of this work are threefold:

- To improve the spatial resolution of five images obtained using different technologies: *QuickBird*, *IKONOS*, *Landsat-7*, *Landsat-8* and an Intergraph Z/I-Imaging digital mapping camera.
- To implement in the form of an open source program three pan-sharpening algorithms (high-pass filter, principal component analysis and Gram–Schmidt transformation) and two quality indices for the pan-sharpened images (spectral ERGAS (*Erreur Relative Globale Adimensionnelle de Synthèse*) index, and ERGAS spatial index). Implementing the abovementioned algorithms as open source is one of our research objectives since it facilitates transparency: open source software implies that all of the code within a given workflow is completely visible to the users. There are no hidden processes or black boxes (Hengl, McMillan, & Wheeler, 2018).
- To discuss the advantages and deficiencies of each pan-sharpening method in each of the study areas and sensors used.

2 | MATERIALS AND METHODS

2.1 | Analyzed images

Figure 1 shows two maps identifying the locations which the images represent: one map with four images located between southern Ecuador and northern Peru (Figure 1a) and the other with the NATMUR-08 image in south-eastern Spain (Figure 1b). The images were captured by sensors from five different platforms, and their main characteristics are shown in Table 1.

QuickBird was a commercial satellite launched on October 18, 2001, in a heliosynchronous orbit (450 and 482 km altitude). It had two charge-coupled device cameras, one PAN and one MS (blue (B), green (G), red (R), and near infrared (NIR) bands). The sweeping width covered by these images was between 16.8 and 18 km, depending on the orbital height (Digital Globe, 2013b). The satellite was deactivated in 2015, 2.5 years after its expected activity end date.

The *QuickBird* image analyzed covers an area of 4.63 km^2 and corresponds to the city of Azogues (Ecuador), including part of the Burgay River which runs north–south. Several characteristic spots such as the Central Plaza,

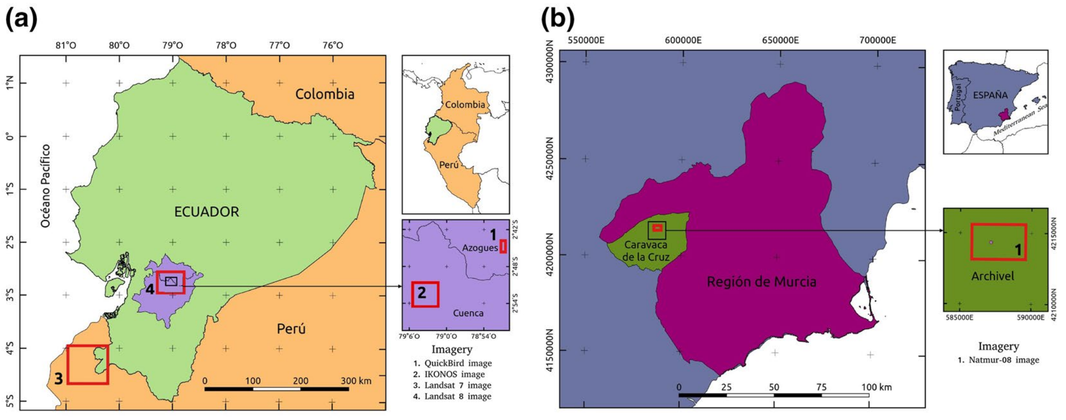

FIGURE 1 Locations of the images used in this work: (a) Ecuador and Peru; and (b) Spain

TABLE 1 Main characteristics of the analyzed images

Platform	Spatial res. (m) MS, PAN	Spectral res. sensor, fused	Radiometric res. (bits)	No. of rows (PAN)	No. of columns (PAN)	EPSG code
QuickBird	2.4, 0.6	4, 4	11	5,677	2,267	32717
IKONOS	4, 1	4, 4	11	6,109	5,300	32717
Landsat-7	30, 15	7,4	8	5,544	5,823	32717
Landsat-8	30, 15	10,3	16	2,977	3,736	32617
Airbone sensor	2, 0.45	4, 4	12	5,451	8,401	25830

Abbreviations: EPSG, European Petroleum Survey Group; res., resolution.

the Cuenca–Azogues highway, the bus station and the municipal stadium can be distinguished in the image. A subset of this is shown in Figure 2a.

IKONOS was a commercial Earth observation satellite launched on September 24, 1999. It was the first satellite to make high-resolution images available to the public, constituting a milestone in remote sensing. In orbit at 681 km, the width of the images was 11 km (Digital Globe, 2013a). In January 2015, DigitalGlobe, the owner of the satellite, announced that, due to problems with quality standards, the satellite had been deactivated.

The *IKONOS* image analyzed (32.4 km^2) covers the western edge of the city of Cuenca and some small towns surrounding the city. Land use basically corresponds to buildings, crops, forests, and shrubs. A subset of the PAN image is shown in Figure 2b.

Landsat-7 and *Landsat-8* are part of a constellation of eight satellites that have provided Earth surface information since 1972. The Landsat project has been one of the most successful space remote sensing projects developed to date (Chuvieco, 2016). The images used in this work were:

- *Landsat-7* image corresponding to the continental part of image P011R063 acquired on October 25, 2001. It covers an area of 6,555 km^2, and includes the southwestern part of the Province of Loja (cantón Zapotillo, Ecuador) and part of the departments of Tumbes and Piura in Peru. There are no major urban centers such as provincial or departmental capitals. Most of the region is made up of dry forests, arid zones, and small cultivated areas. This image shows the Pozos Dam, which is part of the Chira-Piura Irrigation Project in Peru. A subset of the image is presented in Figure 2c.
- *Landsat-8* image (2,502 km^2) corresponding to a part of image P010R062 acquired on October 30, 2014. It covers the cities of Cuenca and Azogues, as well as the Cajas National Park. It is possible to distinguish a large area of the Andean *paramo* in the Ecuadorian Western Cordillera as well as urban zones, arable land, and forests. Figure 2d shows a subset of the original PAN image.

The application of pan-sharpening algorithms near the Equator has been poorly documented in scientific work. Almost all research on this subject uses images of places located at mid-latitudes. In low latitudes, the almost total absence of cloudless days makes it difficult to obtain optical images, which was an added difficulty in carrying out this research.

The NATMUR-08 project was a technical assistance programme carried out on behalf of the Murcia regional government (Spain), which involved taking digital photogrammetric images by airborne PAN and MS (R, G, B, NIR bands) sensors (Intergraph Z/I-Imaging digital mapping camera), and a LiDAR survey for the generation of digital terrain models. The project generated PAN images with a spatial resolution of 0.45 m and MS images with a spatial resolution of 2 m. The size of the image used was 5,451 rows by 8,401 columns (9.27 km^2) and covers the hamlet of Archivel, belonging to the municipality of Caravaca de la Cruz, in the region of Murcia. A subset of the image is presented in Figure 2e.

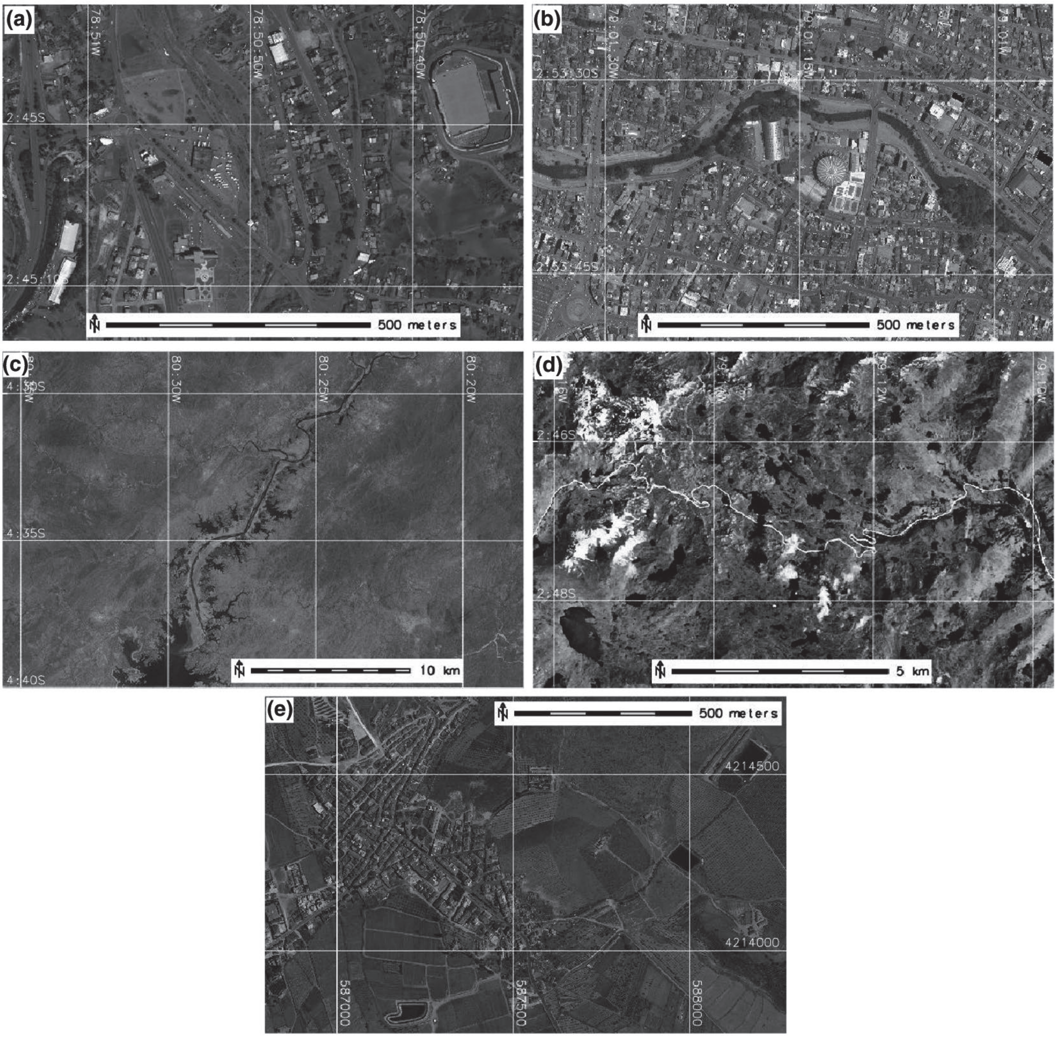

FIGURE 2 Clips of the analyzed images: (a) *QuickBird*; (b) *IKONOS*; (c) *Landsat-7*; (d) *Landsat-8*; and (e) NATMUR-08

These images were chosen because they represent different combinations of terrestrial coverage and different sensors (four satellite-based platforms and one airborne). The resolution characteristics (spectral, spatial, radiometric) of the sensors made it possible to apply the three pan-sharpening techniques to images that represent, in our opinion, a wide range of available resolutions. The spatial ratios of the images are shown in Table 2. This ratio is much higher for images of very high spatial resolution (*QuickBird*, *IKONOS*, and NATMUR-08) than for images of medium spatial resolution (*Landsat-7* and *Landsat-8*).

2.2 | Image pan-sharpening methods

Ideally, a good pan-sharpening method should not only increase the spatial resolution of MS data, but also preserve, as far as possible, its spectral integrity (Chavez, Stuart, & Anderson, 1991; Laben & Brower, 2000; Ranchin & Wald, 2000). It can be concluded from Liu and Mason (2009) that color distortion can be significant if the

TABLE 2 Qualitative assessment according to spectral criteria (brightness and existence of anomalous colors) and spatial criteria (sharpness of the edges and spatial contrast between different elements of the scene) after visual interpretation of Figures 4–13

		Spectral criteria			Spatial criteria		
Image	Figure	HPF	PCA	GS	HPF	PCA	GS
Quickbird	4	5	4	5	5	5	5
	5	5	4	4	5	4	5
IKONOS	6	5	4	5	5	5	5
	7	5	5	5	4	5	5
Landsat 7	8	4	3	3	4	4	4
	9	5	4	4	4	4	4
Landsat 8	10	4	4	5	5	5	5
	11	4	4	5	5	5	5
Natmur-08	12	5	4	5	5	5	5
	13	5	5	5	5	5	5

Note: 1 = very bad; 2 = bad; 3 = acceptable; 4 = good; 5 = very good.
Abbreviations: GS, Gram–Schmidt; HPF, high-pass filter pan-sharpening; PCA, principal component analysis.

spectral range of the MS bands is different from that of the PAN band. Taking these considerations into account, we have only performed pan-sharpening in the MS bands covered by the PAN and in those bands beyond the PAN that are highly correlated with the MS bands covered by the PAN. This is a somewhat less restrictive criterion than that used by Švab and Oštir (2006) who claim that the spectral bands used in pan-sharpening should cover the same wavelengths as the PAN band, and should follow a similar sensitivity to that of the sensor.

Three current pan-sharpening algorithms are implemented: high-pass filter, principal component analysis, and Gram–Schmidt transformation. The reasons for choosing these are that they have produced appropriate results in previous studies, that they represent the main types of image pan-sharpening techniques (Cánovas-García & Alonso-Sarría, 2014; Gangkofner et al., 2008; Karathanassi, Kolokousis, & Ioannidou, 2007; Sarp, 2014; Yuhendra et al., 2010; Zhang & Mishra, 2012), and that they are considered by several authors as state-of-the-art pan-sharpening methods (Snehmani et al., 2016; Vivone et al., 2015).

The high-pass filter (HPF), which is a space domain image pan-sharpening technique, inserts high-frequency components into images of low spatial resolution. The HPF methodology was introduced by Schowengerdt (1980) as a data reconstruction and compression technique, and has been extended to new data sets to fuse images of different spatial and spectral resolutions (Chavez, Guptill, & Bowell, 1984; Cliche, Bonn, & Teillet, 1985; Chavez et al., 1991). According to Gangkofner et al. (2008), this technique has generally been implemented in a simplistic manner because the parameters used have not been optimized to achieve satisfactory spatial and radiometric results. The same authors proposed an optimization and standardization of the method in order to guarantee its applicability to a wide range of images with different ratios between the MS and PAN spatial resolutions (Gangkofner et al., 2008); this standardization method was applied in this research (see online supplementary materials). Although the HPF algorithm implemented in this research dates back to 2008, it is still used with high-spatial-resolution images when pan-sharpening is used as an image preprocessing tool and the objective is land cover classification (Ghosh & Joshi, 2014).

Principal components analysis (PCA) is considered as a component replacement technique. It involves a linear transformation of the MS bands, the substitution of a variable in the transformed space, and inverse transformation to the original space (Shettigara, 1992). The justification for this substitution is that the PAN image is approximately equal to the first principal component, which contains information that is common to all the bands used as input in the PCA procedure, whereas the spectral information unique to each band is represented in the other components (Chavez et al., 1991). This substitution maximizes the effect of the high-resolution PAN band on the fused bands resulting from the process (Shettigara, 1992). Although the PCA algorithm is one of the oldest and has been widely implemented in many commercial remote sensing packages, it is still used today with appropriate results when the objective is image classification (Gasparovic & Jogun, 2018) or in the restoration of pan-sharpened images (Duran & Buades, 2019).

Gram–Schmidt (GS) transformation, which is also considered a component substitution method (Aiazzi, Baronti, Selva, & Alparone, 2006), was invented by Laben and Brower in 1998 and patented by Eastman Kodak (Laben & Brower, 2000). It is based on the Gram–Schmidt transformation, a vector orthogonalization process. In the case of images, each band corresponds to a high-dimensional vector, and these are rotated to produce a new set of uncorrelated vectors (Maurer, 2013). The algorithm is still used in specific pan-sharpening research. For example, Du, Younan, King, and Shah (2007) compared Brovey, GS, PCA, a multiplicative method, and UNB PanShapr pan-sharpening techniques on *QuickBird* and *IKONOS* images and concluded that GS was among the methods that produced the best results. Karathanassi et al. (2007) compared intensity, hue and saturation transformation, Brovey, PCA, GS, and local mean and variance matching and concluded that GS was one of the most efficient methods. Finally, Jawak and Luis (2013), after comparing six methods, concluded that GS produced the best results. The GS pan-sharpening procedure, summarized in five steps, can be consulted in detail in Laben and Brower (2000) and in the online supplementary materials.

Our intention, therefore, was to use well-known algorithms that have been well tested on a real application, without resorting to newer algorithms that have recently been shown to provide appropriate experimental results but which have hardly been used in remote sensing applications. In addition, our aim was to equate the functionalities that exist in free geospatial software with those in two of the most widely used proprietary remote sensing programs today, ENVI and ERDAS Imagine (2013 versions).

Details of the R implementation of the three algorithms can be found in the online supplementary materials.

2.3 | Image pan-sharpening assessment

Two evaluation approaches (qualitative and quantitative) were followed, both commonly used in pure and practical image pan-sharpening research (Belfiore, Meneghini, Parente, & Santamaria, 2016; Kaplan, 2018; Pohl & Van Gendreen, 1998; Vivone et al., 2015).

There are no standard protocols for the visual evaluation of image pan-sharpening, although some criteria have been proposed (European Commission, 1994; Lu, Algazi, & Estes, 1996; Shi, Zhu, Tian, & Nichol, 2005; Wald, Ranchin, & Mangolini, 1997). This work takes into account spectral and spatial criteria. The spectral criteria we considered are brightness, evaluating the perceptible intensity differences of a certain color between the original and the fused image, and anomalous colors, taking into account variations of color between both images. As regards spatial criteria, the fused image should maintain the sharpness of an object's outline and the spatial contrast between different elements without producing veined textures in the form of small elongated distortions that sometimes appear when a pan-sharpening algorithm is applied.

As the evaluation of the visual quality of merged images has a subjective component, it is important to ensure that the display conditions (monitor, histogram stretch, etc.) are consistent (Zhang, 2008). In any case, the bias and experience of the evaluator will inevitably affect the evaluation (Ehlers & Astrand, 2008; Fonseca et al., 2011; Jagalingam & Hegde, 2015; Klonus & Ehlers, 2009; Wang, Ziou, Armenakis, Li, & Li, 2005). The thematic application must also be considered in relation to the aim of the fusion (Pellemans, Jordans, & Allewn, 1993; Wald et al., 1997), which will condition the perception of the evaluator (Wald et al., 1997).

Ten mosaics (Figures 4–13), two for each sensor, containing a clip of the image in its original version, HPF pan-sharpened, PCA pan-sharpened, and GS pan-sharpened were composed to perform the evaluation presented in Table 2. The clips selected were those with the most pronounced spectral contrast among the objects. For each case a color composition was used to highlight these contrasts. When possible, the same color composition was used for data obtained from the same sensor. Only when the contrast of the two images was not clear enough to recognize differences did we use two different compositions for the data of the same sensor. To evaluate the mosaics, they were displayed with a linear adjustment of the histogram between the minimum and maximum percentiles (0.5 and 99.5%, respectively) for all bands. A five-point scale was used to assess the quality of the compositions: 1 = very bad, 2 = bad, 3 = acceptable, 4 = good, 5 = very good. A qualitative assessment of the entire scene analyzed was not considered feasible due to the time involved—for example, about 350 clips similar to the *IKONOS* image would need to be analyzed to cover the entire merged scene. In addition, the subjectivity of this type of validation could make the evaluation process infeasible.

Pan-sharpening may cause alterations in the radiometry of the image that may be not visually perceivable, but enough to invalidate further analysis, such as atmospheric corrections or the estimation of variables. This is why, although necessary, visual assessment is not sufficient. An example of such alterations was described by Zhang (2008).

The quantitative evaluation was carried out using two algorithms: the spectral ERGAS index (or ERGAS index) and the spatial ERGAS index. We are aware that some researchers have used a large number of quality indices (Snehmani et al., 2016; Vivone et al., 2015). However, without wishing to suggest that such an approach is not appropriate, we stress that the goal of the present research was to provide remote sensing practitioners with a powerful, but also rapid and efficient computation tool, for which reason we opted for the simplest quantitative evaluation possible.

The spectral ERGAS index, proposed by Wald (2000, 2002), was used to compare the spectral quality of the pan-sharpened images. The three main requirements of this index are: independence from the units, that is, radiance values or quantities without units; independence from the number of bands in the image to be pan-sharpened; and independence from the spatial resolution ratio between the MS and the PAN images. To calculate this index in full resolution mode, the original MS bands are downscaled (DsMS) to the spatial resolution of the pan-sharpened bands (fused multispectral (FMS) bands). We shall call this the *full resolution* analysis.

The *frERGAS* index (Equation 2) uses the full resolution root mean square error, given by:

$$frRMSE=\sqrt{\frac{1}{P}\sum_{p=1}^{P}(DsMS_p-FMS_p)^2}, \quad (1)$$

to measure the extent by which two bands differ, where p is each of the individual pixels in the band, P is the total number of pixels in the band, FMS_p is the value of the pixel in the pan-sharpened band and $DsMS_p$ is the value of the pixel in the downscaled multispectral band. Once the *frRMSE* for each band has been obtained, the *frERGAS* index can be calculated:

$$frERGAS=100\frac{r_{pan}}{r_{ms}}\sqrt{\frac{1}{N}\sum_{n=1}^{N}\frac{frRMSE_n^2}{\overline{DsMS}_n^2}} \quad (2)$$

where r_{pan} is the spatial resolution of the panchromatic image, r_{ms} is the spatial resolution of the multispectral image, n refers to each of the multispectral bands involved in the pan-sharpening, N is the number of bands and $\overline{DsMS}_n$ is the arithmetic mean of the downscaled multispectral band n.

The value of ERGAS shows a strong tendency to decrease when the quality of the pan-sharpened product increases. Values less than 3 indicate an acceptable pan-sharpening quality (Ozdarici Ok & Akyurek, 2011; Wald, 2000), which improves as it approaches 0.

The ERGAS index in full resolution mode is necessary to check that there has not been a significant alteration of the radiometric values originally contained in the MS image. However, this is not sufficient on its own because if a new image were to be obtained just by artificially increasing the spatial resolution of the original image (without any pan-sharpening algorithm applied), its ERGAS value would be close to 0, which is the maximum possible. Therefore, other quality measures should be used.

Another way to apply the ERGAS index is to use the *reduced resolution* mode. This consists of upscaling the MS image and the PAN image by applying an equivalent degradation of the spatial ratio; performing the pan-sharpening with these new multispectral and panchromatic images, RMS and RPAN, respectively; and comparing the result (FRMS) with the original multispectral image (MS) using the *rrERGAS* index (ERGAS in reduced resolution mode, Equation 4). The *rrRMSE* is given by:

$$rrRMSE = \sqrt{\frac{1}{P}\sum_{p=1}^{P}(MS_p - FRMS_p)^2}. \tag{3}$$

and then *rrERGAS* is:

$$rrERGAS = 100\frac{r_{ms}}{r_{ms}^2/r_{pan}}\sqrt{\frac{1}{N}\sum_{n=1}^{N}\frac{rrRMSE_n^2}{\overline{MS}_n^2}}. \tag{4}$$

The interpretation of ERGAS in reduced resolution mode is the same as above. The main drawback of this approach is that it assumes that the RMS image is what the sensor would have observed if its spatial resolution were $\frac{r_{ms}^2}{r_{pan}}$ and that RPAN is what the sensor would have observed if its spatial resolution were r_{ms}; something that normally cannot be contrasted. The results of this analysis are sensitive to the method of spatial degradation of images. In our case a 5 × 5 Gaussian filter is applied to resample the MS and PAN images.

Since the ERGAS index only considers the spectral characteristics of the image, Lillo-Saavedra, Gonzalo, Arquero, and Martinez (2005) proposed a new spatial index, called the spatial ERGAS index (Equation 6), also introducing a spatial RMSE:

$$spRMSE = \sqrt{\frac{1}{P}\sum_{p=1}^{P}(AdPAN_p - FMS_p)^2}, \tag{5}$$

where $AdPAN_p$ is each of the pixels of the image obtained by adjusting the histogram of the original panchromatic image to the histogram of the downscaled multispectral band in question. Then

$$spERGAS = 100\frac{r_{pan}}{r_{ms}}\sqrt{\frac{1}{N}\sum_{n=1}^{N}\frac{spRMSE_n^2}{\overline{MS}_n^2}}. \tag{6}$$

We also calculated the running times of the pan-sharpening algorithms on a laptop with an Intel Core i7 64-bit processor, 16 GB of RAM and Xubuntu 16.04 operating system.

A comparison of the fused images in R and proprietary software was also carried out (ERDAS Imagine 2011, hereafter ERDAS; and ENVI 4.7, hereafter ENVI). To this end, the same pan-sharpening was carried out in the respective programs. As regards proprietary software, the HPF pan-sharpening algorithm was run in ERDAS and the PCA and GS algorithms in ENVI. However, for the *IKONOS* and *Landsat-8* images the PCA algorithm was run with ERDAS, since the ENVI results were completely anomalous and therefore impossible to compare. The anomalous results of the ENVI PCA algorithm for the *IKONOS* image are probably related (based on the experience of the authors) to the fact that the algorithm implementing the mathematical transformation obtains a negative first component, which, after the inverse transformation, produces digital numbers very different from those in the original

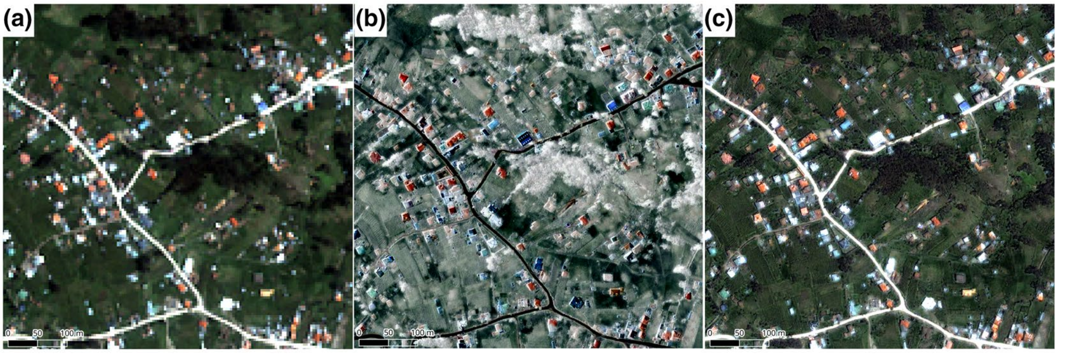

FIGURE 3 Clip of the *IKONOS* image showing some buildings and grassland near the city of Cuenca: (a) original MS image; (b) PCA pan-sharpening implemented in proprietary software (ENVI); and (c) PCA pan-sharpening implemented in R. This location can be visited on Google Earth at https://earth.google.com/web/@-2.92849437,-79.05512228,2706.07174149a,406.44470013d,60y,0h,0t,0r

image (Figure 3). Implementation of the same algorithm produced even stranger results with the *Landsat-8* image, an image in which all pixels have the same value (8,603, 8,905 and 9,071 for the red, green and blue bands, respectively). Since these programs gave consistent results for the pan-sharpening of the other images, it is considered that such anomalies may be associated with characteristics of the original images involved in the pan-sharpening.

HPF pan-sharpening in ERDAS only allows use of the central value options of the filtering matrix (see Section 2.1 of the online supplementary materials) when working with images with a ratio between 1.0 and 2.5. Therefore, for the images with ratios of 4 and 4.4 used in this work the default option was used.

On the other hand, to the best of our knowledge, there is no available commercial software that implements spectral and spatial ERGAS for evaluating the quality of image pan-sharpening, only the freely available software IJFusion (http://ijfusion.es).

Details of the R implementation of the two indices can be found in the online supplementary materials.

2.4 | The fusionImage package

Despite the increasing use of pan-sharpening techniques in remote sensing and of R as data analysis software, no R package implements such techniques and, to the best of our knowledge, only the `RStools` package (Leutner, Horning, & Schwalb-Willmann, 2019) implements PCA pan-sharpening. For this reason, we have created a new R package called `fusionImage` that includes three functions for image pan-sharpening and two functions to assess the quality of a pan-sharpening technique. All functions were programmed using R, so the package works identically on Mac, Windows and GNU/Linux. The package, the manual and some test images are available in the online supplementary materials. Updates of the package will be uploaded to GitHub (http://github.com/pacoalonso/fusionImage). The package has been also submitted to CRAN, the R program repository.

3 | RESULTS AND DISCUSSION

With regard to the qualitative evaluation, all the pan-sharpened images are clearly more helpful for visual interpretation (Figures 4–13). The results presented in Table 2 show how a better qualitative evaluation is obtained in the images with higher spatial ratio between the MS image and the PAN image resolutions (*QuickBird* and *IKONOS* images with spatial resolution ratio of 4 and NATMUR-08 with a ratio of 4.4).

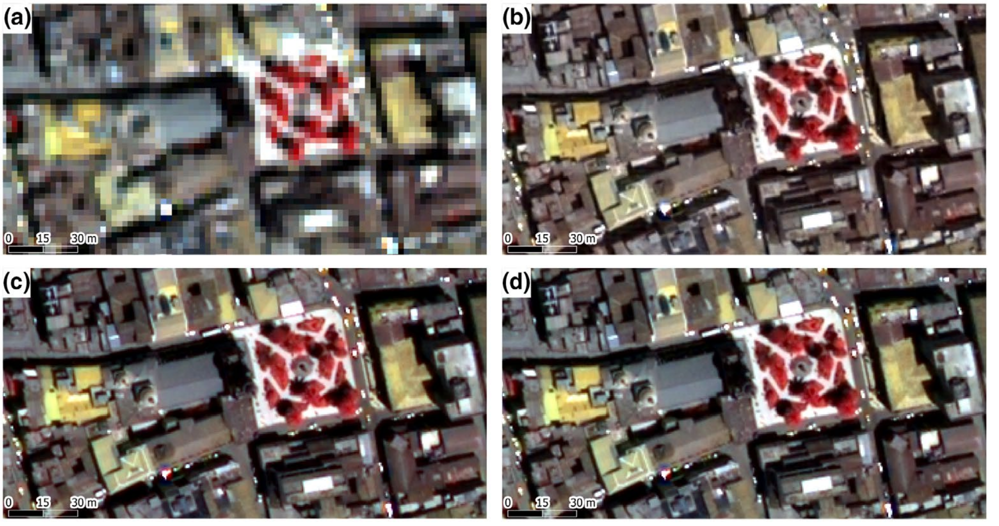

FIGURE 4 Clip of the *QuickBird* image showing the Cathedral of Azoges and Work Park: (a) multi-spectral composite image; (b) HPF pan-sharpening; (c) PCA pan-sharpening; and (d) GS pan-sharpening. This location can be visited on Google Earth at https://earth.app.goo.gl/9Cs7go

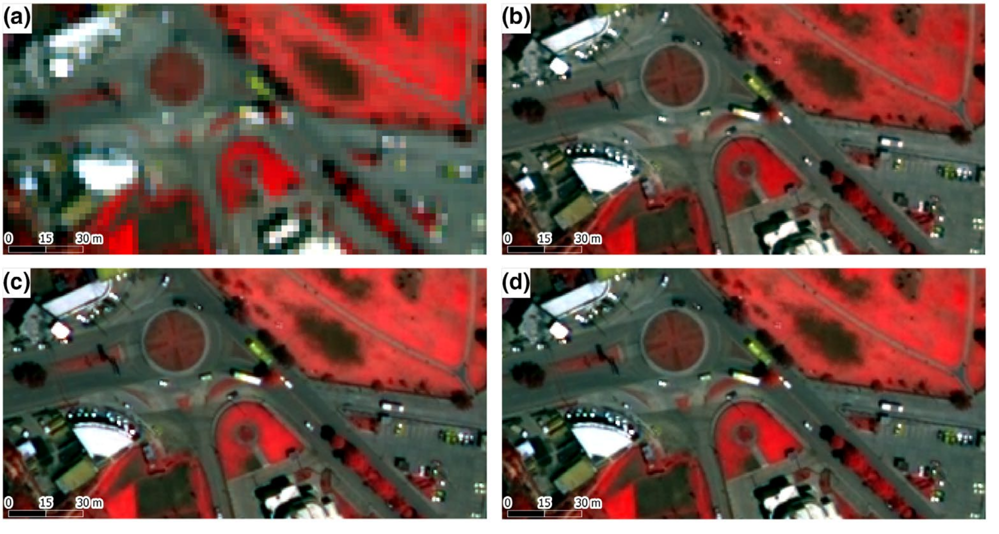

FIGURE 5 Clip of the *QuickBird* image showing a roundabout to access Azogues bus station: (a) multi-spectral composite image; (b) HPF pan-sharpening; (c) PCA pan-sharpening; and (d) GS pan-sharpening. This location can be visited on Google Earth at https://earth.app.goo.gl/?apn=com.google.earth%26ibi=com.google.b612%26isi=293622097%26ius=googleearth%26link=https%253a%252f%252fearth.google.com%252fweb%252f%2540-2.75038293,-78.84890985,2457.35696742a,304.95154544d,35y,0h,0t,0r

The high visual quality of the images with a spatial resolution ratio of 4 and 4.4 can be partly explained by the visual perception of the degree of improvement in the pan-sharpened images as the spatial ratio increases. This, however, raises the question as to how reliable the pan-sharpening between MS and PAN images would be at a larger spatial ratio (the present research uses images with ratios lower than or equal than 4.4).

The *Landsat-7* and *Landsat-8* images show greater color distortion with the three pan-sharpening methods. In the case of the *Landsat-7* images, distortion is smaller when HPF pan-sharpening is used (Figures 8 and 9); on the

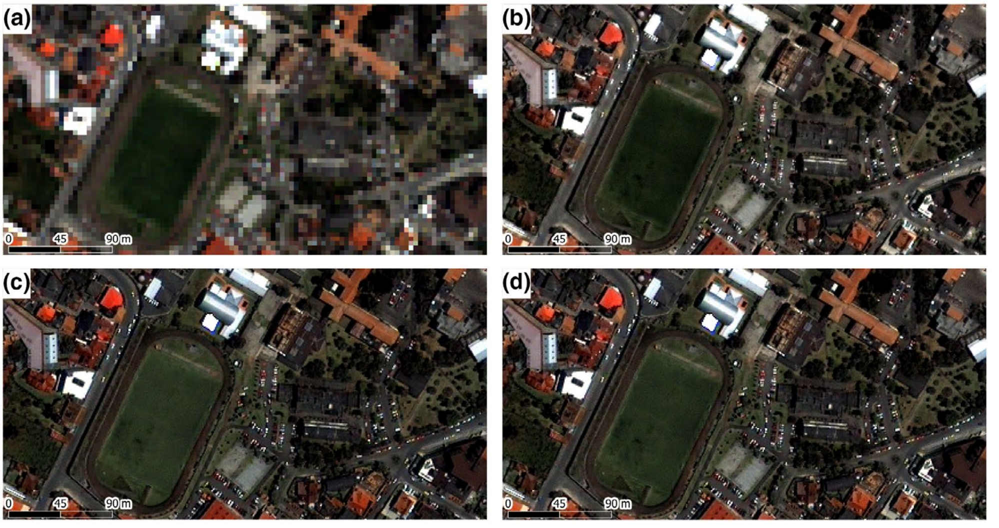

FIGURE 6 Clip of the *IKONOS* image showing the University of Cuenca campus: (a) multi-spectral composite image; (b) HPF pan-sharpening; (c) PCA pan-sharpening; and (d) GS pan-sharpening. This location can be visited on Google Earth at https://earth.app.goo.gl/?apn=com.google.earth%26ibi=com.google.b612%26isi=293622097%26ius=googleearth%26link=https%253a%252f%252fearth.google.com%252fweb%252f%2540-2.90190713,-79.00995892,2530.76653708a,370.90379843d,35y,0h,0t,0r

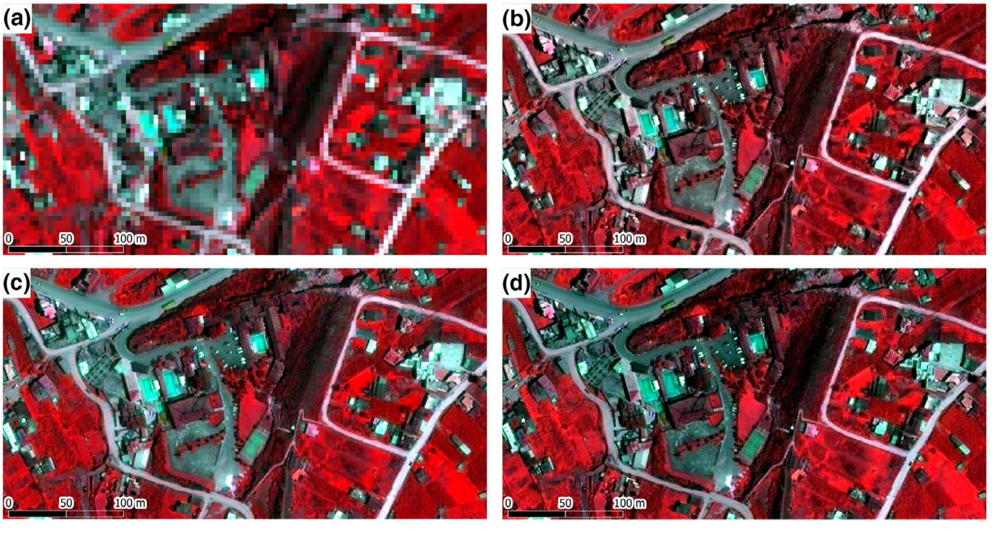

FIGURE 7 Clip of the *IKONOS* image showing Baños-Cuenca water pools: (a) multi-spectral composite image; (b) HPF pan-sharpening; (c) PCA pan-sharpening; and (d) GS pan-sharpening. This location can be visited on Google Earth at https://earth.app.goo.gl/eNR1tC

other hand, for the *Landsat-8* images, the GS pan-sharpening produces the lowest distortion (Figures 10 and 11). The qualitative evaluation reveals better results for the *QuickBird*, *IKONOS*, and NATMUR-08 images, especially with HPF and GS, both in spectral and spatial terms.

Turning to the quantitative evaluation (Figure 14), the results show that no pan-sharpening method obtains optimal results simultaneously for all the images used. The best results for *frERGAS* were obtained with HPF pan-sharpening in the *QuickBird* and *Landsat-7* images, followed by GS pan-sharpening. This is important,

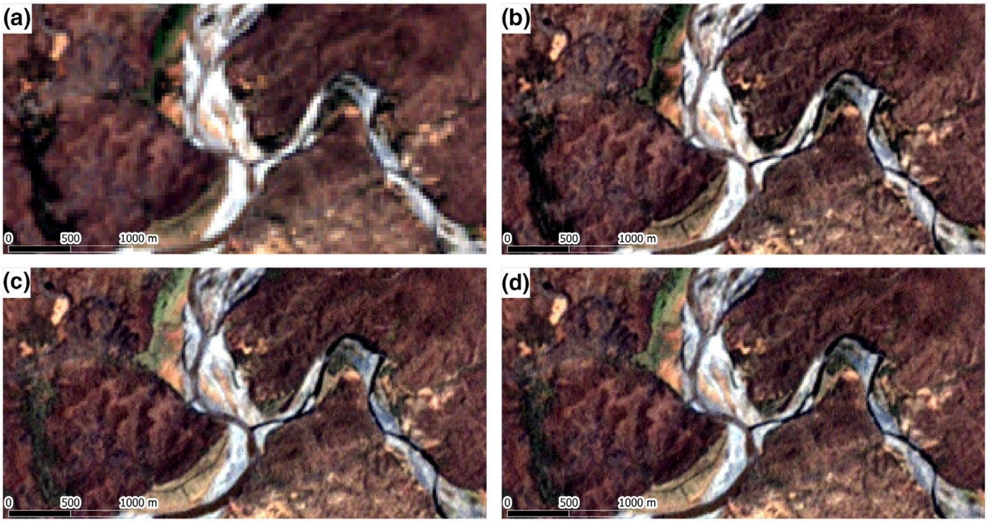

FIGURE 8 Clip of the *Landsat-7* image showing a segment of the River Chira and one of its tributaries, 10 km downstream from Zapotillo: (a) multi-spectral composite image; (b) HPF pan-sharpening; (c) PCA pan-sharpening; and (d) GS pan-sharpening. This location can be visited on Google Earth at https://earth.app.goo.gl/kLy1z4

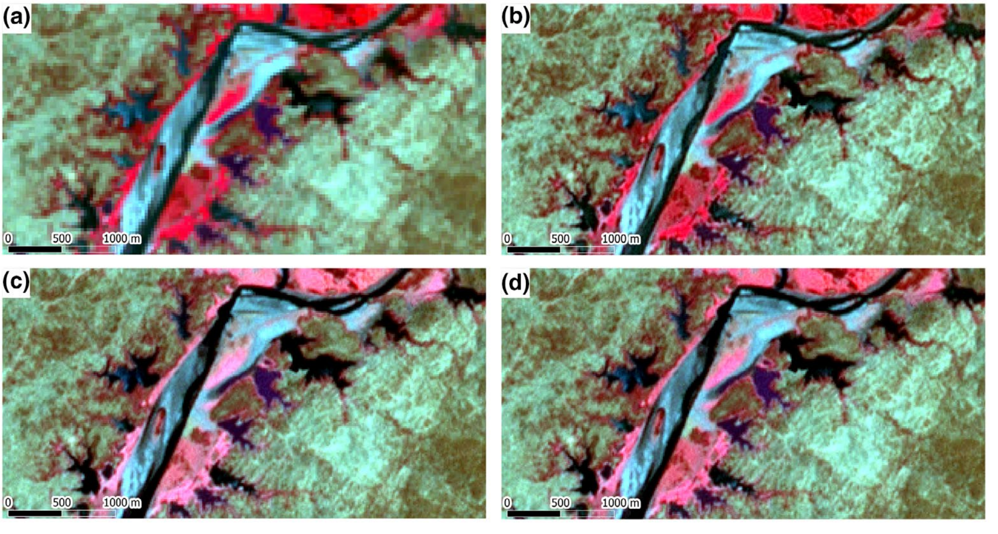

FIGURE 9 Clip of the *Landsat-7* image showing the tail of the Poechos-Perú reservoir: (a) multi-spectral composite image; (b) HPF pan-sharpening; (c) PCA pan-sharpening; and (d) GS pan-sharpening. This location can be visited on Google Earth at https://earth.google.com/web/@-4.55818624,-80.44681148,111.48618934a,8581.46351617d,35y,0h,0t,0r

considering that the HPF algorithm is based on map algebra operations, which makes its implementation simpler compared with other methodologies, and it also takes less time to obtain the merged bands (Table 3). However, in the case of the *Landsat-8* and NATMUR-08 images, the results are much more even. As regards the GS pan-sharpening method, the simulated PAN band that is used as the first band for the Gram–Schmidt transformation was calculated as the average of all the MS bands used. However, it could be calculated by weighting the original MS

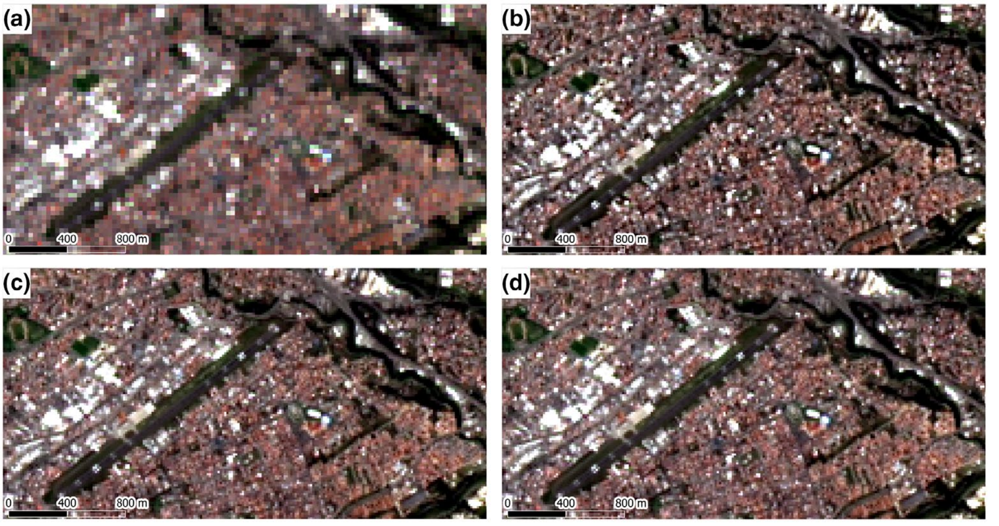

FIGURE 10 Clip of the *Landsat-8* image showing Mariscal La Mar Cuenca Airport: (a) multi-spectral composite image; (b) HPF pan-sharpening; (c) PCA pan-sharpening; and (d) GS pan-sharpening. This location can be visited on Google Earth at https://earth.app.goo.gl/?apn=com.google.earth%26ibi=com.google.b612%26isi=293622097%26ius=googleearth%26link=https%253a%252f%252fearth.google.com%252fweb%5C%252f%5C%2540-2.88876854,-78.97763918,2511.32021931a,2806.19391048d,35y,0h,2.68601361t,0r

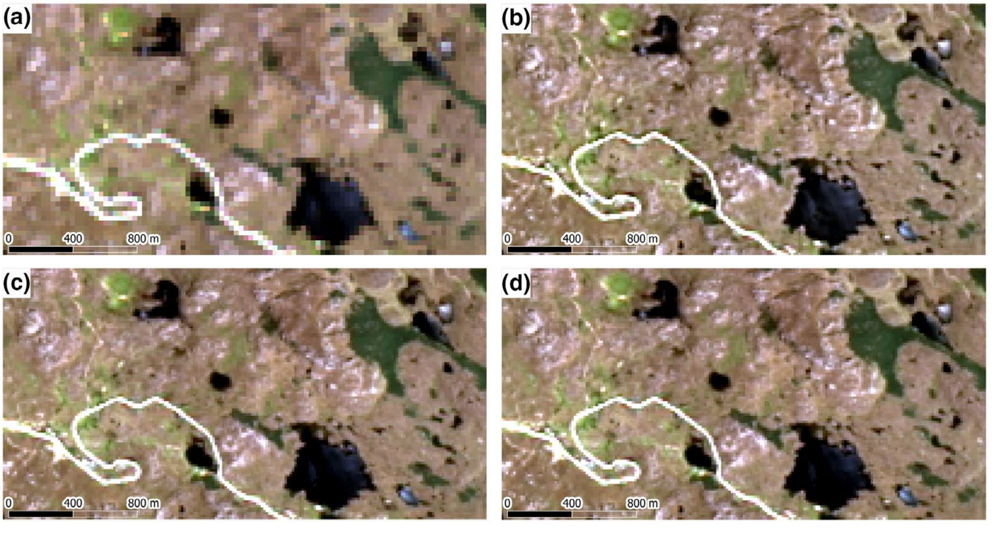

FIGURE 11 Clip of the *Landsat-8* image showing the Cajas National Park, Toreadora lagoon and Cuenca–Guayaquil road: (a) multi-spectral composite image; (b) HPF pan-sharpening; (c) PCA pan-sharpening; and (d) GS pan-sharpening. This location can be visited on Google Earth at https://earth.app.goo.gl/hYUuxM

bands based on the sensor calibration parameters, which, according to Laben and Brower (2000), could improve the pan-sharpening process, although few sensors provide the weighting coefficients. Some studies are even more conclusive and emphasize the most appropriate pan-sharpening method; however, such investigations evaluate just a certain type of image (sensor) (Chavez et al., 1991; Nikolakopoulos, 2008), as opposed to the five types of images used in this research.

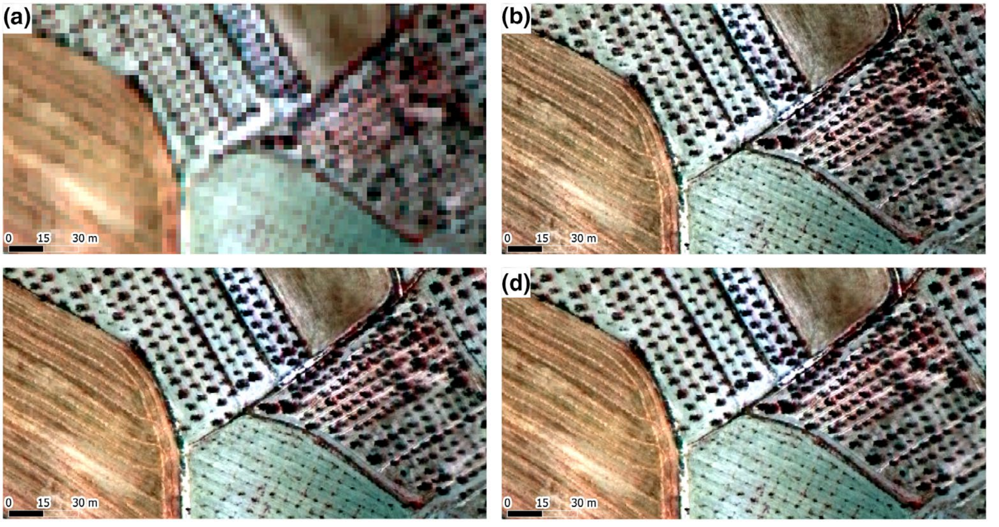

FIGURE 12 Clip of the NATMUR-08 image showing agricultural plots in Archivel (Murcia region): (a) multi-spectral composite image; (b) HPF pan-sharpening; (c) PCA pan-sharpening; and (d) GS pan-sharpening. This location can be visited on Google Earth at https://earth.app.goo.gl/75Dcpd

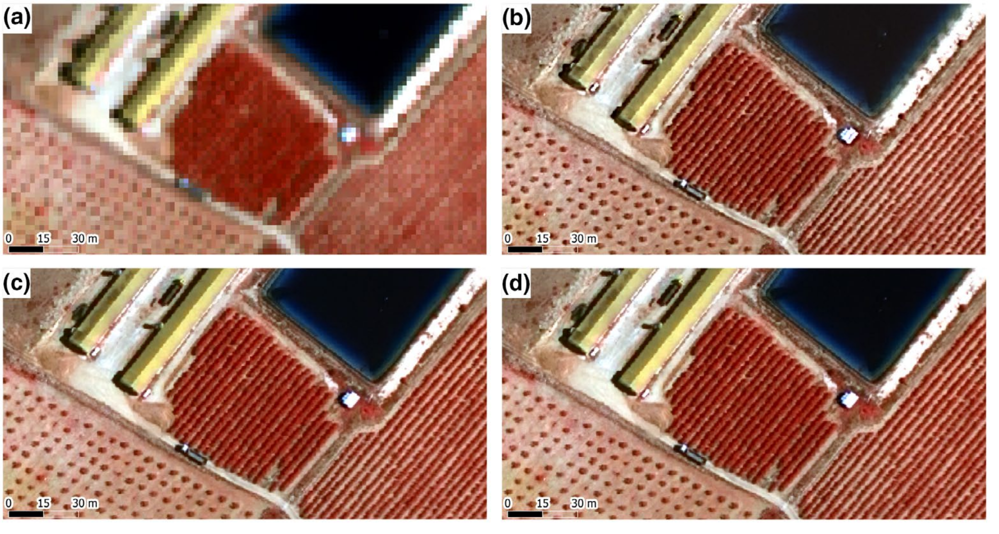

FIGURE 13 Clip of the NATMUR-08 image showing buildings, irrigation pond and trees in Archivel (Murcia region): (a) multi-spectral composite image; (b) HPF pan-sharpening; (c) PCA pan-sharpening; and (d) GS pan-sharpening. This location can be visited on Google Earth at https://earth.app.goo.gl/fKCAYZ

The ERGAS values obtained in reduced resolution mode (*rrERGAS*) are considerably lower than those obtained in full resolution mode, especially at low spatial ratios (*Landsat-7* and *Landsat-8*). Also, there is sufficient coherence in terms of the ERGAS full resolution and ERGAS reduced resolution results, the ranking of the pan-sharpening algorithms being similar in both modes.

With regard to the spatial ERGAS index, PCA pan-sharpening was the best option for the *QuickBird*, *Landsat-7* and *Landsat-8* images, followed by GS. With respect to the comparatively low ratings obtained for the *QuickBird* and *IKONOS* images with the spatial ERGAS index in the three pan-sharpening methods, it should be noted that

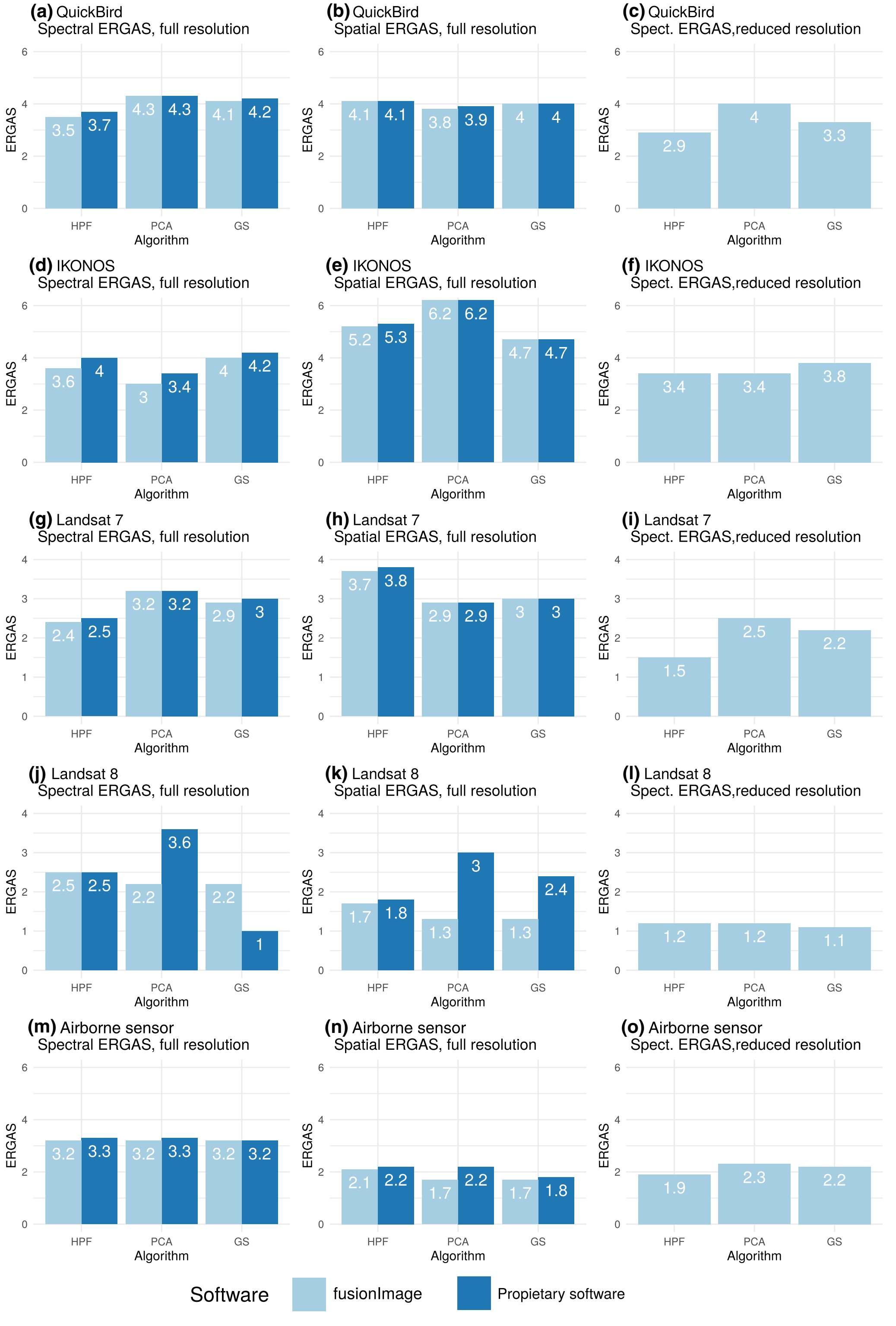

FIGURE 14 Quantitative assessment of the pan-sharpened images. GS, Gram–Schmidt; HPF, high-pass filter pan-sharpening; PCA, principal component analysis

TABLE 3 Performance of the pan-sharpening algorithms implemented in the `fusionImage` package

Platform	No. of pixels per band (Millions)	No. of bands	Seconds HPF	PCA	GS	Seconds/10^6 pix./ band HPF	PCA	GS
QuickBird	12.9	4	35	39	57	0.68	0.7	1.11
IKONOS	32.4	4	82	114	130	0.63	0.88	1.01
Landsat-7	32.3	4	81	100	152	0.63	0.78	1.18
Landsat-8	11.1	3	19	22	33	0.58	0.66	0.98
Airborne sensor	45.8	4	131	431	184	0.72	2.35	1.01

Abbreviations: GS, Gram–Schmidt pan-sharpening; HPF, high=pass filter pan-sharpening; PCA, principal component analysis pan-sharpening.

these two images share two characteristics: a high spatial ratio (4) and the presence of a high percentage of urban coverage. Xu, Zhang, and Li (2014) report that when these two conditions appear simultaneously, a spilling effect frequently occurs due to saturation of the signal during the acquisition phase of MS images as a result of the strong reflectance of some bright objects usually found in urban areas. In this case the fused image, such as the *QuickBird*, would be wrongly evaluated in urban areas (as in our scene) and, in general, in areas with presence of bright objects. This may be the case of the *QuickBird* and *IKONOS* images used in our study.

Four out of the five types of image analyzed show opposite results for spatial and spectral ERGAS. Only in the case of *Landsat-8* does the same algorithm (PCA) obtain better results for spectral and spatial ERGAS. It must be considered that the characteristics of the sensors and the spectral and spatial particularities of each scene or image analyzed make each algorithm respond differently in each case. This shows that it is not possible to identify any of the algorithms analyzed in this research as offering optimal results simultaneously in spectral and spatial terms. This would suggest the existence of a trade-off between the spectral and spatial quality of the pan-sharpened images as suggested by Lillo-Saavedra and Gonzalo (2006), which would lend support to the idea of these authors that incorporating a parameter to modify this trade-off in pan-sharpening algorithms should be considered. In order to elaborate on possible explanations for the variation observed in the results when assessing spectral and spatial components, we believe that a different experimental design is needed. In our case, with the experiments carried out, we can only hypothesize possible causes. The literature in this field points to the effort needed to find the method that best meets the requirements and purposes of any research (Chen, Su, Zhang, Tian, & Yang, 2008; Vivone et al., 2015). In conclusion, there are no better pan-sharpening algorithms, only better pan-sharpened images.

Figure 14c,f,i,l, and o shows the values of spectral and spatial ERGAS in full resolution mode when pan-sharpening is performed with proprietary software. With all the images and pan-sharpening algorithms, except *Landsat-8* and GS, the spectral ERGAS values favor the implementation of R. The same can be said about spatial ERGAS. It is difficult to offer a conclusive explanation since the source code of the proprietary software is not accessible. In the specific case of HPF, ERDAS only allows specific filters for images with a spatial ratio of less than 2.5. This could explain the differences in *QuickBird*, *IKONOS* and NATMUR, but not in *Landsat-7* and *Landsat-8*. The *Landsat-8* case must be analyzed separately, especially taking into account the GS algorithm. Considering only *frERGAS*, it would seem that pan-sharpening with GS in ENVI obtains results (*frERGAS* < 1) that are much better than those obtained with R. However, the spatial ERGAS produces the opposite results if it is compared with spectral ERGAS of GS with R, but in general terms it obtains a quite appropriate value (lower than 2.5). In this case it is necessary to visualize the resulting images (Figure 15), to see that pan-sharpening with proprietary software gave anomalous results, which led to a spurious increase in the spatial resolution without improving its interpretation capacity.

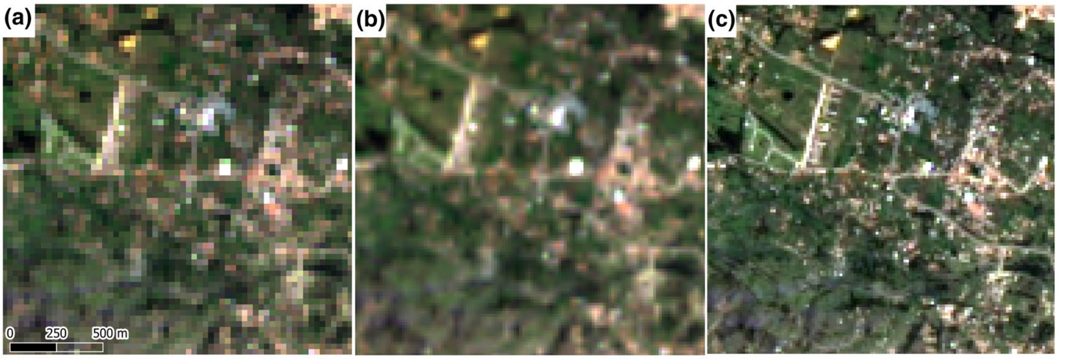

FIGURE 15 Clip of the *Landsat-8* image showing buildings and grassland near the city of Cuenca: (a) original image; (b) GS pan-sharpening implemented in proprietary software (ENVI); and (c) GS pan-sharpening implemented in R. This location can be visited on Google Earth at https://earth.app.goo.gl/uUuAgL

For a detailed quantitative assessment of the pan-sharpened images see Appendix A.

The performance of the pan-sharpening algorithms is presented in Table 3, which, besides the processing time in seconds, presents a computation time indicator expressed in seconds per million pixels per band. According to Table 3 and for the orders of magnitude of the size of the images, it can be claimed that the implementation of the HPF algorithm is the most efficient and the GS algorithm the least. When the number of pixels begins to increase, as in the case of the airborne sensor image, the computation time of the PCA algorithm greatly increases. This behavior is striking, since in the case of *IKONOS* and *Landsat-7* images, processing times increase from about 32 million pixels per band to much less competitive times (four times more) when processing 45.8 million pixels per band (airborne sensor). Taking into account the orders of magnitude considered, when the size of the images increases by 41.3% the processing time increases by more than 400%.

4 | CONCLUSIONS

The objective of this study was threefold: (1) to apply three pan-sharpening image techniques (high-pass filter, principal component analysis and Gram–Schmidt transformation) to fuse MS and PAN images obtained from four satellite platforms (*QuickBird*, *IKONOS*, *Landsat-7* and *Landsat-8*) and an airborne platform with an Intergraph Z/I-Imaging digital mapping camera in order to improve the spatial resolution of the original MS images; (2) to evaluate the results qualitatively by means of a visual comparison, and quantitatively based on two quality indices (the spectral and spatial ERGAS indexes); and (3) to implement these techniques in the form of an open source program.

No qualitatively anomalous results were found in the images resulting from the algorithms implemented in R. However, visually anomalous results were obtained in specific cases when using other programs, as in the examples discussed (Figures 3 and 15).

The qualitative evaluation of the results does not always agree with the quantitative evaluation. Therefore, each of these approaches can provide important analytical information and should be considered in a complementary way when assessing the quality of image pan-sharpening.

According to spectral ERGAS, HPF pan-sharpening offers better results for the *QuickBird* and *Landsat-7* images, PCA for the *IKONOS*, *Landsat-8* and airborne sensor. Although GS obtains appropriate results based on the quantitative evaluation, only once did it obtain the best score based on the spectral index (with *Landsat-8* in reduced resolution mode). This contrast with the results obtained by applying pan-sharpening algorithms with proprietary software, when GS obtained the best values with the spatial index in three of the five images analyzed and was second best in the other two. However, with respect to the spatial ERGAS, GS obtains the best results in three of the five images studied both in the R implementation and with proprietary software.

Any evaluation process has to be applied carefully since significant disagreements may arise if different methods are used. The results of this research indicate that there is a greater consistency when an independent evaluation is carried out for each image, not only because of the characteristics of the sensors themselves, but also because of the different terrain features and environmental factors that affect the images.

R is able to run both simple tasks and complex processes, while maintaining reliability and enabling the implementation of new algorithms such as those proposed in this study. The main problem with R is its limited capability to process large volumes of raster data, although in recent years significant progress has been made in this regard.

This research also offers some results on the computation times used in the processing of each image. This work offers results for images close to the actual application size, while in some previous works computation times are only provided for very small images. The size of the images matters in R and users of this language know that the computation times calculated for small examples are of little use for extrapolation purposes, and that such computation times are only relevant when the architecture of the computer system is known and when images are processed close to the size of real applications. In this sense we have verified that when increasing the size of the images a threshold is reached at which computation times sharply increase, and that the efficiency of the PCA algorithm implementation is reduced considerably when a certain image size is exceeded (possibly around 35 × 4 million pixels). All of this suggests that tools are needed in future versions of the package that allow images to be reduced to tiles before they are processed in parallel, and later joined to form a single image.

Geographers and most Earth, natural and social scientists use data (remote sensing, sensor networks, observatory networks, territorial microdata, big data, etc.) in an intensive way, while open source software is increasingly used to manage these data (Alonso Sarría, Gomariz Castillo, & Cánovas García, 2012). In this respect, computer software has become a key element in research. However concern about the importance of the code has also led to a certain degree of mistrust of proprietary software. Some examples of this have been discussed in this work, but see also Barnes (2010). Rocchini and Neteler (2012) highlights the need to adopt a free software philosophy in ecology, as Alonso Sarría et al. (2012) has done in physical geography and in this work we do for geoinformatics.

The `fusionImage` package endows R, and so provides the GIS and remote sensing research community, with a new set of open source software tools. To the best of our knowledge, there is no open source multiplatform program that implements the three image pan-sharpening algorithms studied in this article, so this contribution helps to reduce the gap in functionality that is only available in proprietary software.

ACKNOWLEDGMENTS

The *QuickBird* image used in this work was provided by the Universidad de las Fuerzas Armadas (Ecuador). The *IKONOS* image from the city of Cuenca was facilitated by the Universidad del Azuay (Ecuador). The NATMUR-08 image was provided by the CARM Environmental Integration and Management Service (Murcia region, Spain). We sincerely thank these three institutions for permission to use the images. Fulgencio Cánovas-García thanks Gema González Romero and Juan Carlos Rodríguez Mateos from the University of Seville (Spain) for their help in several teaching activities. Without their help it would have been almost impossible to complete this work. We also thank the anonymous reviewers, whose suggestions substantially improved the original manuscript.

CONFLICT OF INTEREST

The authors declare no conflict of interest.

ORCID

Fulgencio Cánovas-García https://orcid.org/0000-0002-9188-3202
Francisco Alonso-Sarría https://orcid.org/0000-0003-0466-5184

REFERENCES

Aiazzi, B., Baronti, S., Selva, M., & Alparone, L. (2006). Enhanced Gram-Schmidt spectral sharpening based on multivariate regression of MS and pan data. In *Proceedings of the IGARSS IEEE Geoscience and Remote Sensing Symposium*, Denver, CO (pp. 3806–3809). Piscataway, NJ: IEEE.

Alonso Sarría, F., Gomariz Castillo, F., & Cánovas García, F. (2012). Conocimiento abierto en sistemas de información geográfica. Una estrategia para la geografía física. *Nimbus: Revista de Climatología, Meteorología y Paisaje*, *29–30*, *21–34*. Retrieved from https://dialnet.unirioja.es/servlet/articulo?codigo=4375477

Amro, I., Mateos, J., Vega, M., Molina, R., & Katsaggelos, A. K. (2011). A survey of classical methods and new trends in pansharpening of multispectral images. *EURASIP Journal on Advances in Signal Processing*, *2011*, 79.

Barnes, N. (2010). Publish your computer code: It is good enough. *Nature*, *467*, 753.

Basaeed, E., Bhaskar, H., & Al-Mualla, M. (2013). Comparative analysis of pan-sharpening techniques on DubaiSat-1 images. In *Proceedings of the 16th International Conference on Information Fusion*, Instanbul, Turkey (pp. 227–234). Piscataway, NJ: IEEE.

Belfiore, O. R., Meneghini, C., Parente, C., & Santamaria, R. (2016). Application of different pan-sharpening methods on WorldView-3 images. *ARPN Journal of Engineering & Applied Sciences*, *11*(1), 490–496.

Bivand, R. S., Pebesma, E. J., & Gómez-Rubio, V. (2013). *Applied spatial data analysis with R* (2nd ed.). Berlin, Germany: Springer. Retrieved from https://www.springer.com/gp/book/9781461476177

Brodu, N. (2017). Super-resolving multiresolution images with band-independent geometry of multispectral pixels. *IEEE Transactions on Geoscience & Remote Sensing*, *55*, 4610–4617.

Cánovas-García, F., & Alonso-Sarría, F. (2014). Comparación de técnicas de fusión en imágenes de alta resolución espacial. *GeoFocus*, *14*, 144–162.

Chavez, P., Guptill, S., & Bowell, J. (1984). Image processing techniques for Thematic Mapper data. In *Proceedings of the 50th Annual ASP-ACSM Symposium*, Washington, DC (Technical Papers, Vol. 2, pp. 728–742). Bethesda, MD: American Society of Photogrammetry.

Chavez, P., Stuart, C., & Anderson, J. (1991). Comparison of three different methods to merge multiresolution and multispectral data: Landsat TM and SPOT panchromatic. *Photogrammetric Engineering & Remote Sensing*, *57*, 295–303.

Chen, S., Su, H., Zhang, R., Tian, J., & Yang, L. (2008). The tradeoff analysis for remote sensing image fusion using expanded spectral angle mapper. *Sensors*, *8*, 520–528.

Chuvieco, E. (2016). *Fundamentals of satellite remote sensing. An environmental approach* (2nd ed.). Boca Raton, FL: CRC Press. https://doi.org/10.1111/phor.12184

Cliche, C., Bonn, F., & Teillet, P. (1985). Integration of the SPOT panchromatic channel into its multispectral mode for image sharpness enhancement. *Photogrammetric Engineering & Remote Sensing*, *51*, 311–316.

Darvishi Boloorani, A. (2008). *Remotely sensed data fusion as a basis for environmental studies: Concepts, techniques and applications* (Unpublished PhD dissertation). University of Göttingen, Göttingen, Germany.

Digital Globe. (2013a). *IKONOS (Data sheet)*. Retrieved from https://dg-cms-uploads-production.s3.amazonaws.com/uploads/document/file/96/DG_IKONOS_DS.pdf

Digital Globe. (2013b). *QuickBird (Data sheet)*. Retrieved from https://dg-cms-uploads-production.s3.amazonaws.com/uploads/document/file/100/QuickBird-DS-QB-Prod.pdf

Du, Q., Younan, N., King, R., & Shah, V. (2007). On the performance evaluation of pan-sharpening techniques. *IEEE Geoscience & Remote Sensing Letters*, *4*, 518–522.

Duran, J., & Buades, A. (2019). Restoration of pansharpened images by conditional filtering in the PCA domain. *IEEE Geoscience & Remote Sensing Letters*, *16*, 442–446.

Ehlers, M., & Astrand, P. J. (2008). Quality assessment for multi-sensor multi-date image fusion. *International Archives of Photogrammetry, Remote Sensing & Spatial Information Sciences*, *37*(WG IV/4), 3797–3803.

Ehlers, M., Jacobsen, K., & Schiewe, J. (2009). High resolution image data and GIS. In M. Madden (Ed.), *Manual of geographic information systems* (pp. 721–777). Bethesda, MD: American Society for Photogrammetry and Remote Sensing.

Ehlers, M., Klonus, S., Astrand, P., & Rosso, P. (2010). Multi-sensor image fusion for pansharpening in remote sensing. *International Journal of Image & Data Fusion*, *1*, 25–45.

European Commission. (1994). *CORINE land cover. Technical guide*. Luxembourg: Office for Official Publications of European Communities.

Ewertowski, M. W., Evans, D. J. A., Roberts, D. H., & Tomczyk, A. M. (2016). Glacial geomorphology of the terrestrial margins of the tidewater glacier, Nordenskiöldbreen, Svalbard. *Journal of Maps*, *12*, 476–487.

Fonseca, L., Namikawa, L., Castejon, E., Carvalho, L., Pinho, C., & Pagamisse, A. (2011). Image fusion for remote sensing applications. In Y. Zheng (Ed.), *Image fusion and its applications* (pp. 153–178). London, UK: IntechOpen.

Gangkofner, U. G., Pradhan, P. S., & Holcomb, D. W. (2008). Optimizing the high-pass filter addition technique for image fusion. *Photogrammetric Engineering & Remote Sensing*, *74*, 1107–1118.

Gasparovic, M., & Jogun, T. (2018). The effect of fusing Sentinel-2 bands on land-cover classification. *International Journal of Remote Sensing*, *39*(3), 822–841.
Ghosh, A., & Joshi, P. (2014). A comparison of selected classification algorithms for mapping bamboo patches in lower Gangetic plains using very high resolution WorldView 2 imagery. *International Journal of Applied Earth Observation & Geoinformation*, *26*, 298–311.
Goslee, S. C. (2011). Analyzing remote sensing data in R: The Landsat package. *Journal of Statistical Software*, *43*, 1–25.
Hengl, T., McMillan, B. A., & Wheeler, I. (2018). A brief introduction to open data, open source software and collective intelligence for environmental data creators and users. *PeerJ Preprints*, *6*, e27127v1.
Hijmans, R. J. (2016). *raster: Geographic data analysis and modeling*. Retrieved from https://cran.r-project.org/web/packages/raster/index.html
Huang, X., Wen, D., Li, J., & Qin, R. (2017). Multi-level monitoring of subtle urban changes for the megacities of China using high-resolution multi-view satellite imagery. *Remote Sensing of Environment*, *196*, 56–75.
Jagalingam, P., & Hegde, A. V. (2015). A review of quality metrics for fused image. *Aquatic Procedia*, *4*, 133–142.
Jawak, S. D., & Luis, A. J. (2013). A comprehensive evaluation of pan-sharpening algorithms coupled with resampling methods for image synthesis of very high resolution remotely sensed satellite data. *Advances in Remote Sensing*, *2*, 332–344.
Kaplan, G. (2018). Sentinel-2 pan sharpening: Comparative analysis. *Multidisciplinary Digital Publishing Institute Proceedings*, *2*(7), 345.
Karathanassi, V., Kolokousis, P., & Ioannidou, S. (2007). A comparison study on fusion methods using evaluation indicators. *International Journal of Remote Sensing*, *28*, 2309–2341.
Klonus, S., & Ehlers, M. (2009). Performance of evaluation methods in image fusion. In *Proceedings of the 12th International Conference on Information Fusion*, Seattle, WA (pp. 1409–1416). Piscataway, NJ: IEEE.
Laben, C., & Brower, B. (2000). *Process for enhancing the spatial resolution of multispectral imagery using pan-sharpening* (U.S. Patent 6,011,875). Alexandria, VA: US Patent and Trademark Office. Retrieved from https://www.lens.org/lens/patent/US_6011875_A
Leutner, B., Horning, N., & Schwalb-Willmann, J. (2019). *RStoolbox: Tools for remote sensing data analysis*. Retrieved from https://CRAN.R-project.org/package=RStoolbox. R package version 0.2.6.
Lillo-Saavedra, M., & Gonzalo, C. (2006). Spectral or spatial quality for fused satellite imagery? A trade-off solution using the wavelet *á trous* algorithm. *International Journal of Remote Sensing*, *27*, 1453–1464.
Lillo-Saavedra, M., Gonzalo, C., Arquero, A., & Martinez, E. (2005). Fusion of multispectral and panchromatic satellite sensor imagery based on tailored filtering in the Fourier domain. *International Journal of Remote Sensing*, *26*, 1263–1268.
Liu, J., & Mason, P. (2009). *Essential image processing and GIS for remote sensing*. Oxford, UK: Wiley-Blackwell. https://doi.org/10.1002/9781118687963
Lu, J., Algazi, V. R., & Estes, R. R. (1996). Comparative study of wavelet image coders. *Optical Engineering*, *35*, 2605–2620.
Maurer, T. (2013). How to pan-sharpen images using the Gram-Schmidt pan-sharpen method: A recipe. *ISPRS International Archives of Photogrammetry, Remote Sensing & Spatial Information Sciences*, *41*(1/W1), 239–244.
Nikolakopoulos, K. G. (2008). Comparison of nine fusion techniques for very high resolution data. *Photogrammetric Engineering & Remote Sensing*, *74*, 647–659.
Ozdarici Ok, A., & Akyurek, Z. (2011). Evaluation of image fusion methods on agricultural lands. *Journal of Earth Science & Engineering*, *1*, 107–113.
Pebesma, E. (2018). Simple features for R: Standardized support for spatial vector data. *The R Journal*, *10*, 439–446.
Pebesma, E., Nüst, D., & Bivand, R. (2012). The R software environment in reproducible geoscientific research. *Eos*, *93*, 163–164.
Pellemans, A. H. J. M., Jordans, R. W. L., & Allewn, R. (1993). Merging multispectral and panchromatic spot images with respect to the radiometric properties of the sensor. *Photogrammetric Engineering & Remote Sensing*, *59*, 81–87.
Pohl, C., & Van Gendreen, J. (1998). Multisensor image fusion in remote sensing: Concepts, methods and applications. *International Journal of Remote Sensing*, *19*, 823–854.
R Development Core Team. (2009). *R: A language and environment for statistical computing*. Vienna, Austria: R Foundation for Statistical Computing.
Ranchin, T., & Wald, L. (2000). Fusion of high spatial and spectral resolution images: The ARSIS concept and its implementation. *Photogrammetric Engineering & Remote Sensing*, *66*, 49–61.
Rocchini, D., & Neteler, M. (2012). Let the four freedoms paradigm apply to ecology. *Trends in Ecology & Evolution*, *27*, 310–311.
Sarp, G. (2014). Spectral and spatial quality analysis of pan-sharpening algorithms: A case study in Istanbul. *European Journal of Remote Sensing*, *47*, 19–28.
Schowengerdt, R. (1980). Reconstruction of multispatial, multispectral image data using spatial frequency content. *Photogrammetric Engineering & Remote Sensing*, *46*, 1325–1334.

Shettigara, V. (1992). A generalized component substitution technique for spatial enhancement of multispectral images using a higher resolution data set. *Photogrammetric Engineering & Remote Sensing*, *58*, 561–567.

Shi, W., Zhu, C., Tian, Y., & Nichol, J. (2005). Wavelet-based image fusion and quality assessment. *International Journal of Applied Earth Observation & Geoinformation*, *6*, 241–251.

Snehmani, A. G., Ganju, A., Kumar, S., Srivastava, P. K., & Hari Ram, R. P. (2016). A comparative analysis of pansharpening techniques on Quickbird and WorldView-3 images. *Geocarto International*, *32*, 1268–1284.

Švab, A., & Oštir, K. (2006). High-resolution image fusion: Methods to preserve spectral and spatial resolution. *Photogrammetric Engineering & Remote Sensing*, *72*, 565–572.

Vivone, G., Alparone, L., Chanussot, J., Dalla Mura, M., Garzelli, A., Licciardi, G. A., ... Wald, L. (2015). A critical comparison among pansharpening algorithms. *IEEE Transactions on Geoscience & Remote Sensing*, *53*, 2565–2586.

Wald, L. (2000). Quality of high resolution synthesised images: Is there a simple criterion? In T. Ranchin & L. Wald (Eds.), *Proceedings of the Third Conference on Fusion of Earth Data: Merging Point Measurements, Raster Maps and Remotely Sensed Images*, Sophia Antipolis, France (pp. 99–103). Nice, France: SEE/URISCA.

Wald, L. (2002). *Data fusion: Definitions and architectures*. Paris, France: Presses de l'Ecole, Ecole des Mines de Paris.

Wald, L., Ranchin, T., & Mangolini, M. (1997). Fusion of satellite images of different spatial resolutions: Assessing the quality of resulting images. *Photogrammetric Engineering & Remote Sensing*, *63*, 691–699.

Wang, Z., Ziou, D., Armenakis, C., Li, D., & Li, Q. (2005). A comparative analysis of image fusion methods. *IEEE Transactions on Geoscience & Remote Sensing*, *43*, 1391–1402.

Xu, Q., Zhang, Y., & Li, B. (2014). Recent advances in pansharpening and key problems in applications. *International Journal of Image & Data Fusion*, *5*, 175–195.

Yokoya, N., Grohnfeldt, C., & Chanussot, J. (2017). Hyperspectral and multispectral data fusion: A comparative review of the recent literature. *IEEE Geoscience & Remote Sensing Magazine*, *5*, 29–56.

Yuhendra, H., Kuze, H., & Sri Sumantyo, J. (2010). Performance analyzing of high resolution pan-sharpening techniques: Increasing image quality for classification using supervised kernel support vector machine. In H. Fejita & J. Sewald (Eds.), *Selected topics in power systems and remote sensing* (pp. 260–268). Athens, Greece: WSEAS Press.

Zhang, H., & Roy, D. (2016). Computationally inexpensive Landsat 8 operational land imager (OLI) pansharpening. *Remote Sensing*, *8*, 180.

Zhang, Y. (2002). Problems in the fusion of commercial high-resolution satellite images as well as Landsat 7 images and initial solutions. In *Proceedings of the ISPRS Symposium on Geospatial Theory, Processing, and Applications*, Ottawa, Canada. Retrieved from https://www.isprs.org/proceedings/xxxiv/part4/pdfpapers/220.pdf

Zhang, Y. (2004). Understanding image fusion. *Photogrammetric Engineering & Remote Sensing*, *70*, 657–661.

Zhang, Y. (2008). Methods for image fusion quality assessment: A review, comparison and analysis. *ISPRS International Archives of Photogrammetry, Remote Sensing & Spatial Information Sciences*, *37*, 1101–1109.

Zhang, Y., & Mishra, R. K. (2012). A review and comparison of commercially available pan-sharpening techniques for high resolution satellite image fusion. In *Proceedings of the 32nd Geoscience and Remote Sensing Symposium*, Munich, Germany (pp. 182–185). Piscataway, NJ: IEEE.

SUPPORTING INFORMATION

Additional supporting information may be found online in the Supporting Information section.

How to cite this article: Cánovas-García F, Pesántez-Cobos P, Alonso-Sarría F. fusionImage: An R package for pan-sharpening images in open source software. *Transactions in GIS*. 2020;24:1185–1207. https://doi.org/10.1111/tgis.12676

APPENDIX A

DETAILED QUANTITATIVE ASSESSMENT OF THE PAN-SHARPENED IMAGES

TABLE A1 Detailed quantitative assessment of the pan-sharpened images

Band	Spectral ERGAS DsMS vs. FMS Full resolution			Spatial ERGAS AdPAN vs. FMS Full resolution			Spectral ERGAS MS vs. FRMS Reduced resolution			Spectral ERGAS DsMS vs. PrFMS Full resolution			Spatial ERGAS AdPAN vs. PrFMS Full resolution		
QuickBird															
	HPF	PCA	GS	HPF	PCA	GS	HPF	PCA	GS	HPF	PCA	GS	HPF	PCA	GS
1	3.04	3.85	3.59	3.69	2.63	3.05	2.57	3.61	3.02	3.21	3.87	3.72	3.75	2.70	3.04
2	3.43	4.55	4.25	3.62	2.03	2.63	2.84	4.03	3.33	3.66	4.58	4.39	3.69	2.09	2.61
3	4.36	5.68	5.30	4.57	3.12	3.84	3.47	4.95	4.04	4.60	5.64	5.41	4.66	3.22	3.83
4	3.02	2.27	2.55	4.23	6.09	5.77	2.78	3.06	2.71	3.23	2.66	2.75	4.32	6.12	5.78
Global	**3.51**	4.27	4.05	4.05	**3.80**	4.01	**2.93**	3.97	3.31	**3.72**	4.33	4.18	4.13	**3.85**	4.00
IKONOS															
1	5.08	3.95	5.66	7.61	9.21	6.35	4.92	4.85	5.41	5.70	4.63	6.00	7.77	9.28	6.32
2	3.44	2.97	4.07	4.49	5.43	3.31	3.06	3.07	3.51	3.83	3.29	4.24	4.59	5.48	3.29
3	2.73	2.03	2.95	4.25	5.10	3.59	2.66	2.62	2.95	3.16	2.42	3.16	4.34	5.13	3.57
4	2.79	2.73	2.51	3.31	3.59	4.84	2.48	2.46	2.41	2.68	2.95	2.84	3.41	3.52	4.83
Global	3.63	**3.00**	3.98	5.17	6.19	**4.68**	3.42	**3.39**	3.75	4.01	**3.42**	4.24	5.29	6.22	**4.66**
Landsat-7															
1	1.62	2.16	1.96	2.97	1.88	2.01	1.16	1.83	1.60	1.70	2.20	2.05	3.05	1.87	2.02
2	2.48	3.40	3.11	3.55	1.83	2.00	1.55	2.72	2.35	2.57	3.43	3.19	3.66	1.83	2.02
3	3.16	4.37	3.98	4.54	1.91	2.56	1.94	3.48	3.00	3.25	4.40	4.06	4.65	1.91	2.60
4	1.88	2.10	2.00	3.39	4.86	4.62	1.20	1.61	1.46	1.98	2.13	2.04	3.47	4.85	4.61
Global	**2.36**	3.15	2.89	3.66	**2.92**	3.00	**1.50**	2.52	2.19	**2.45**	3.18	2.96	3.75	2.92	**3.01**
Landsat-8															
1	2.26	1.97	1.99	1.68	1.39	1.33	1.16	1.02	0.99	2.30	3.25	0.79	1.83	2.80	2.49
2	2.37	2.08	2.11	1.38	1.02	1.00	1.20	1.15	1.12	2.42	3.44	0.92	1.57	2.80	2.21
3	2.71	2.39	2.42	1.85	1.54	1.62	1.31	1.33	1.29	2.78	3.94	1.15	2.03	3.36	2.53
Global	2.45	**2.15**	2.18	1.65	**1.34**	**1.34**	1.22	1.17	**1.14**	2.51	3.55	**0.97**	**1.82**	3.00	2.41
Airborne sensor															
1	3.74	3.73	3.76	2.00	1.27	1.41	2.13	2.62	2.57	3.83	3.83	3.80	2.08	2.08	1.44
2	3.32	3.33	3.37	1.78	1.03	1.03	1.88	2.30	2.26	3.42	3.42	3.37	1.85	1.85	1.07
3	3.16	3.07	3.12	2.37	2.06	2.00	1.91	2.22	2.19	3.26	3.26	3.12	2.43	2.43	2.03
4	2.59	2.42	2.46	2.15	2.25	2.20	1.59	1.80	1.78	2.66	2.66	2.50	2.20	2.20	2.22
Global	3.23	**3.17**	3.21	2.09	1.73	**1.72**	**1.89**	2.25	2.22	3.32	3.32	**3.23**	2.15	2.15	**1.75**

Note: Values in bold indicate which method obtained the best result according to ERGAS.
Abbreviations: ERGAS, *Erreur Relative Globale Adimensionnelle de Synthèse*; GS, Gram–Schmidt; HPF, high-pass filter pan-sharpening; PCA, principal components analysis.

AdPAN, adjusted panchromatic image; FMS, fused multispectral image; FRMS, fused-reduced multispectral image; full resolution, same resolution as panchromatic image; MS, multispectral image; PrFMS, fused multispectral image with proprietary software; reduced resolution, same resolution as multispectral image.